Optical imaging with spectrum aberration correction using a filtering macrolens

Yu-Hsuan Lin,[1,2,*] Jyun-Yi Lai,[1] Hsin-Yi Tsai,[1] Han-Chao Chang,[1] Hung Ji Huang,[1] Yung-Fu Chen,[2] and Kuo-Cheng Huang[1]

[1]Instrument Technology Research Center, National Applied Research Laboratories, Hsinchu 30076, Taiwan

[2]Department of Electrophysics, National Chiao Tung University, Hsinchu 30010, Taiwan

*Corresponding author: marklin@itrc.narl.org.tw

Received 6 May 2013; revised 12 June 2013; accepted 13 June 2013;
posted 14 June 2013 (Doc. ID 189993); published 11 July 2013

A filtering macrolens was developed to simultaneously achieve macro-optical imaging and correct spectrum aberration. The macrolens was a doublet lens comprising a filtering lens and a close-up lens. The shape of the filtering lens was designed to eliminate the optical path differences between the light rays in the absorbing medium. The close-up lens was designed to decrease the effective focal length of an ordinary camera lens to provide high magnification capability and collimate the diverging beams through the filtering lens. Experimental results demonstrated that the spectrum uniformity of the macro-optical images was markedly improved by the filtering macrolens. This innovation may be used in finite conjugate optical systems.

OCIS codes: (090.1000) Aberration compensation; (220.3620) Lens system design; (350.2450) Filters, absorption.

http://dx.doi.org/10.1364/AO.52.005058

1. Introduction

The absorbing filter is an optical element used to isolate specific regions of a spectrum. It is a powerful tool and has been widely used for light attenuation and spectral selection of a broadband light source in filters such as neutral density (ND) filters, colored glass filters, and dichroic filters. The extent of absorption of light by an absorbing filter varies with the wavelength of the light and the thickness of the filter. In general, the thicker the filter material, the wider the range of wavelengths it will absorb. The Beer–Lambert–Bouguer law governs the progressive weakening of a monochromatic beam of light being propagated in a homogeneous absorbing medium [1–3]. The logarithmic relationship between the internal transmission at various wavelengths and the distance traveled by the light in the material can be expressed as follows:

$$\tau(\lambda) = 10^{-\alpha(\lambda)l}, \tag{1}$$

where l is the optical path length (OPL), and $\alpha(\lambda)$ is the absorption coefficient of the filter material and can be expressed in terms of the imaginary part of the refractive index and the free-space wavelength of the light [4,5]. The internal spectral transmission $\tau(\lambda)$ describes the transmission of the absorbing filter without considering reflection losses. Taking reflection losses into account yields the external spectral transmission $T(\lambda)$, which is the product of the internal spectral transmission and the reflection factor.

For various thicknesses of the absorbing filter, the Beer–Lambert–Bouguer law for normal incident radiation can be written as follows [6,7]:

$$T_1(\lambda) = P(\lambda) \cdot \tau_2(\lambda)^{\frac{d_1}{d_2}}, \tag{2}$$

where $P(\lambda)$ is the spectral reflection factor, which can be quantified by the Fresnel equation [8]; $T_1(\lambda)$

1559-128X/13/215058-07$15.00/0

is the external transmission at wavelength λ and with a filter thickness d_1; and $\tau_2(\lambda)$ is the internal transmission at wavelength λ and with a filter thickness d_2. When the filter thicknesses are equal, the external transmissions will also be equal ($d_1 = d_2$, $T_1(\lambda) = P(\lambda) \cdot \tau_2(\lambda) = T_2(\lambda)$). The Beer–Lambert–Bouguer law is precise only when the power density of the incident beam is lower than a few kilowatt [9].

Equation (2) illustrates the dependence of the external spectral transmission on filter thickness for normal incident radiation. To provide uniform spectral characteristics, optical filters are typically produced as flat pieces with uniform thickness. However, scenarios that involve diverging or converging source beams are ignored. As shown in Fig. 1, when noncollimated beams pass through a normal filter, the OPL varies with the incident or divergent angles. Therefore, absorption differences occur, which leads to the relatively poor uniformity of the spectral transmission. This may be regarded as a spectrum aberration, illustrating that normal filters may work effectively in infinite conjugate optical systems but not in finite conjugate optical systems.

In this study, a filtering macrolens was developed to achieve macro-optical imaging and perform the function of an ND filter and an edge pass filter with superior optical qualities. The macrolens was a doublet lens composed of a meniscus-absorbing filter lens and a double-convex neutral glass lens. The shape of the absorbing filter lens was designed to eliminate optical path differences (OPDs) between beams traveling through the medium. The shape of the neutral glass lens was designed to collimate the light beams coming through the absorbing filter and to provide a macroimaging function [10]. As with normal filters, the filtering macrolens can be mounted on the thread of an ordinary camera lens. The macrolens provides a finite conjugate optical system with high magnification capability and high spectrum uniformity for macrophotography. This study presents a solution to provide simple, low-cost optical filters that show favorable aberration correction, uniform optical density, and high compatibility with ordinary camera lenses.

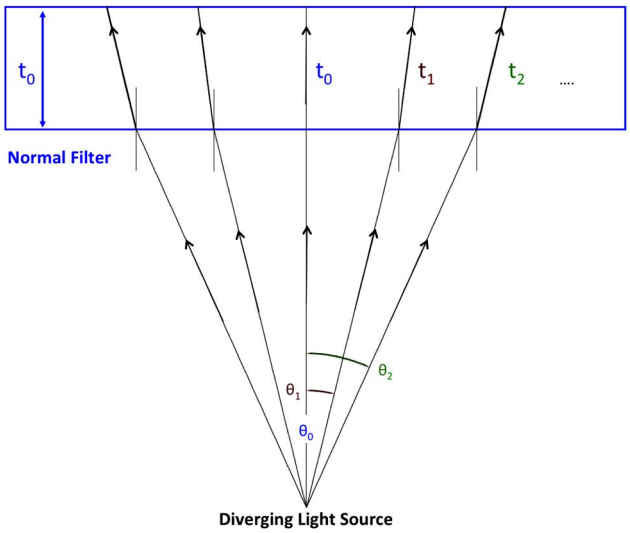

Fig. 1. Thickness of a normal absorbing filter is constant (t_0). When diverging light beams enter the filter medium, the OPL increases ($t_2 > t_1 > t_0$) with increasing divergence angle ($\theta_2 > \theta_1 > \theta_0$). According to the Beer–Lambert–Bouguer law, the optical density changes and spectral red-shift occurs. The reflection loss also increases with increasing divergence angle. These effects cause poor uniformity of the spectral transmission.

2. Theoretical Analysis

The filtering macrolens is an optical device made up of two paired singlet lenses—a filtering lens and a close-up lens. The filtering lens element is a type of absorbing filter shaped into a meniscus for spectrum aberration correction. The spectrum characteristics of the filtering lens depend on the material of the absorbing filter. In this paper, a long pass glass filter (OG530, Schott AG, Germany) was used [11]. The close-up lens element was a neutral glass shaped into a symmetrical double convex. The close-up lens decreases the effective focal length (EFL) of the camera lens and allows the camera to be positioned closer to the subject [12]. In this section, the radii of the curvature and thickness of these two lens elements are calculated using geometric optics and Optalix simulation. The improvement in spectrum aberration of the various filtering lenses is analyzed numerically.

A. Meniscus Filtering Lens

The optical model of the filtering lens is illustrated in Fig. 2. The filtering lens has two radii of curvature, which have the same value R_c. The centers of curvature of the two radii are located at points A and O. The displaced distance between two curved surfaces along the optical axis is represented as t_0 (lens center displacement), so that $\overline{AO} = t_0$. The light ray originates from point C with a divergence angle θ, and

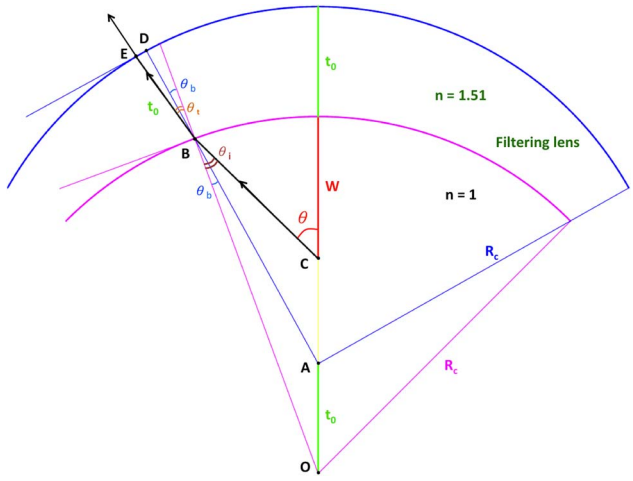

Fig. 2. Optical model of the meniscus filtering lens. The light ray starts from point C with a divergence angle θ. It enters the lens at point B and leaves at point E. For ideal spectrum aberration correction, the traveling distance of the light in the medium must be equal to the lens center displacement t_0.

the working distance of the lens is defined as W. Refraction occurs at the first surface boundary (point B) of the lens for the incident light, where $\overline{OB}$ is the direction of the normal. The Snell law provides the relationship between the angles of incidence and refraction:

$$n \cdot \sin \theta_t = n_0 \cdot \sin \theta_i, \tag{3}$$

where θ_i and θ_t are the incident and refractive angle, respectively; n is the refractive index of the lens material, which is equal to 1.51; and n_0 is the refractive index of the ambient medium (air), which is equal to 1. The next refraction occurs at the second surface boundary (point E) and the light ray subsequently travels into air. To acquire the constant OPL at any incidence angle, the $\overline{BE}$ must be constrained to equal t_0. For convenience, the $\angle ABO$ is labeled θ_b. The divergence angle θ is an external angle of the triangle BOC; therefore $\angle COB = \theta - \theta_i$.

The distance $\overline{CO}$, one side of the triangle BOC, can be derived as a function of R_c, θ, and θ_i. The working distance W can be obtained by subtracting $\overline{CO}$ from the radius of curvature R_c. Therefore, W can further be expressed as

$$W = R_c \cdot \left[1 - \frac{\tan \theta_i \cdot (1 + \tan \theta \cdot \tan \theta_i)}{\tan \theta \cdot (1 + \tan^2 \theta_i) \cdot \cos(\theta - \theta_i)}\right]. \tag{4}$$

The angle θ_b is one angle of the triangle AOB and can be derived as a function of R_c, θ, θ_i, and t_0:

$$\theta_b = \tan^{-1}\left(\frac{t_0 \cdot \sin \cdot \theta - \theta_i)}{R_c - t_0 \cdot \cos(\theta - \theta_i)}\right). \tag{5}$$

Figure 2 shows that $\overline{BD}$ is equal to $\overline{AD} - \overline{AB}$, where $\overline{AD} = R_c$, and $\overline{AB}$ is one side of the triangle AOB and can be derived as a function of R_c, θ, θ_i, and θ_b. Therefore, the $\overline{BD}$ can be expressed as

$$\overline{BD} = R_c\left\{1 - \frac{1}{\cos \theta_b} \cdot \left[1 - \frac{\tan \theta_b}{\tan \theta_b + \tan(\theta - \theta_i)}\right]\right. . \tag{6}$$

If the radius of the curvature is considerably larger than the lens center displacement ($R_c \gg t_0$), then $\overline{BD}$ can be expressed as

$$\overline{BD} \cong \overline{BE} \cdot \cos(\theta_t - \theta_b) = t_o \cdot \cos(\theta_t - \theta_b). \tag{7}$$

In this paper, the lens center displacement t_0 and the working distance W were set as 3 and 60 mm, respectively. The divergence angle θ was limited to 60°. The relationship between the radius of curvature R_c and the divergence angle θ can be acquired simultaneously by solving Eqs. (3)–(7). The numerical values of R_c and θ were obtained using a Mathematica 8.0 (Wolfram Research, 2010) calculation. The relationship is plotted as the dashed curve in Fig. 3.

The results showed that the radius of curvature R_c increased nonlinearly with increasing divergence angle θ. The extreme value of R_c was 145 mm at $\theta = 1°$ and 198 mm at $\theta = 60°$. R_c can be any number at $\theta = 0°$ because all the OPLs are equal to the lens center displacement ($t_0 = 3$ mm). The nonlinear variation of R_c means that the filtering lens should be aspherical to perfectly eliminate the OPDs between light beams in the medium. However, aspherical lenses are expensive and difficult to produce. Therefore, as a compromise, the next best design should be considered. The aspherical lens was thus substituted for a spherical lens. As shown by the solid line in Fig. 3, a constant radius of curvature for the spherical lens was chosen, and was expected to eliminate the OPDs to the largest extent.

In Fig. 4, the dependence of the distance that the light travels in the medium on the divergence angle is shown with a normal filter, an aspherical filtering lens, and three spherical filtering lenses with various radii of curvature. The OPDs of the filter and lenses at various divergence angles can be obtained by subtracting the reference length, 3 mm (t_0), from the distance that the light travels in the medium, and taking an absolute value. For a normal filter (curve 1), the OPD rapidly increases with increasing divergence angle, which leads to severe light attenuation and spectral red shift at the edge of the filter. For an aspherical filtering lens (line 2), no OPD exists between the light beams, regardless of the divergence angle. Therefore, the related aberrations can be completely overcome. Regarding the spherical lenses, a filtering lens with a constant radius of curvature of 145 mm (curve 5) has zero OPDs when

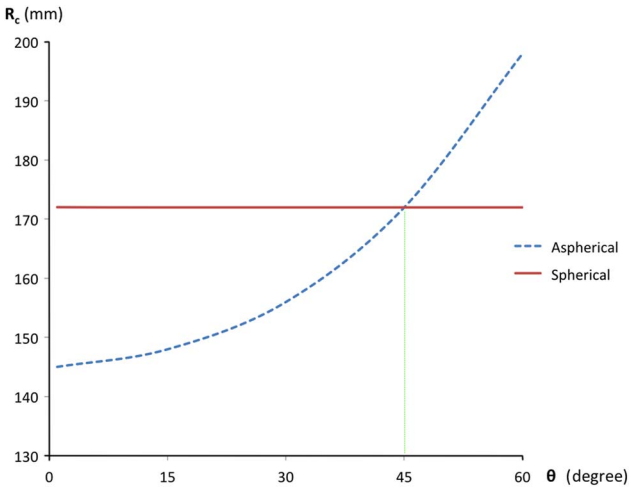

Fig. 3. Radius of the curvature of the filtering lens versus the divergence angles of the light rays for two lens shapes. For prefect spectrum aberration correction, the filtering lens must be aspherical. However, a spherical filtering lens with a suitable radius of curvature can also obtain favorable spectrum aberration correction.

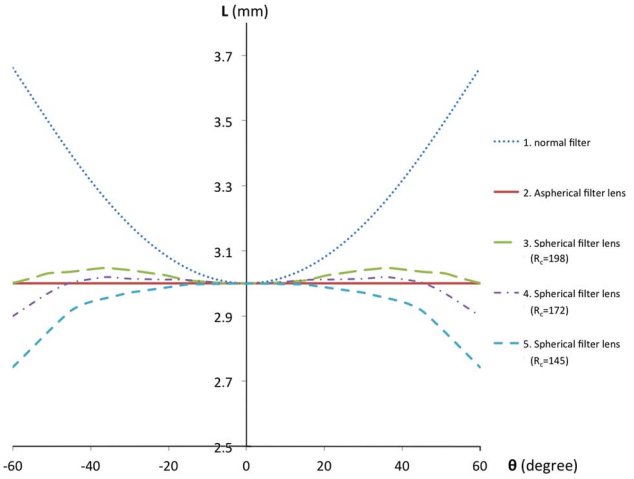

Fig. 4. Illustration of the distance that the light travels in the medium versus the divergence angles of the light rays for the normal filter (curve 1), the aspherical filtering lens (line 2), and the spherical filtering lenses with various radii of curvatures (curves 3–5).

the divergence angle is less than 1°. The OPD gradually decreases with increasing divergence angle when the divergence angle is larger than 1°. Therefore, higher transmission and spectral blue shift occurs at the edge of the lens. A filtering lens with a constant radius of curvature of 198 mm (curve 3) has zero OPDs only at the divergence angles of 0° and 60°. The curve resembles a small hill and the OPD reaches its peak at a divergence angle of approximately 35°. Therefore, maximal light attenuation and spectral red shift occurs at a distance approximately equal to half the radius of the lens. To ensure a spherical filtering lens with center-weighted uniformity, a filter lens with a constant radius of curvature of 172 mm (curve 4) was chosen, which provided favorable spectrum aberration correction when the divergence angle was less than 45°, and acceptable spectrum aberration when the divergence angle was larger than 45°.

The external transmissions of the normal filter and the filtering lenses are not only related to OPD, but also to the reflection factor. Because of reflection at the two glass-air interfaces of each filter or lens, the optical intensities are attenuated. The Fresnel equation is used to calculate the reflectance at the two interfaces of an optical device [8,13]. If the incident light is unpolarized, the reflectance at any wavelength is

$$R_{\text{unpolarised}} = \frac{R_s + R_p}{2}, \tag{8}$$

where R_s, R_p is the reflectance of the s-polarized light and the p-polarized light, respectively. They are given by

$$R_s = \left| \frac{n_1 \cdot \cos\,\theta_i - n_2 \cdot \cos\,\theta_t}{n_1 \cdot \cos\,\theta_i + n_2 \cdot \cos\,\theta_t} \right|^2 \tag{9}$$

$$R_s = \left| \frac{n_1 \cdot \cos\,\theta_t - n_2 \cdot \cos\,\theta_i}{n_1 \cdot \cos\,\theta_t + n_2 \cdot \cos\,\theta_i} \right|^2, \tag{10}$$

where θ_i and θ_t are the incident and refractive angle, respectively, and n_1 and n_2 are the refractive indices of the incident media and refractive media, respectively. The reflection factor P at a specific wavelength can be expressed as

$$P = 1 - R_1 - R_2, \tag{11}$$

where R_1 and R_2 are the reflectance originating from the first and second interface reflections, respectively. Using these equations, the reflection factors of a normal filter and the filtering lenses can be obtained. With an increasing divergence angle of 1°–60°, the reflection factor of a normal filter decreases from 0.92 to 0.82, and the reflection factor of the filtering lens with a radius of curvature of 172 mm decreases from 0.92 to 0.91. This means that the filtering lens provides a more uniform transmission than the normal filter.

Considering the OPDs and reflection factors, the external transmission spectra of the normal filter and the filtering lenses with various divergence angles can be obtained. The normal filter and the filtering lenses were made from long pass glass (OG530, Schott AG, Germany) with a cutoff wavelength λ_c at 530 nm. Figure 5(a) shows the external transmission spectra of the normal filter at divergence angles of 0°, 30°, 45°, and 60°. It is obvious that the light attenuation and red shift both increase with increasing divergence angle. In addition, between the limit of the blocking range and the limit of the pass range, the spectral variation is more sensitive in the long wavelength region than in the short wavelength region. These problems cause color cast and the vignetting effect on macrophotography images. For image analysis in professional research, they may cause more severe mistakes.

Figure 5(b) shows the external transmission spectra of the filtering lens at divergence angles of 0°, 30°, 45°, and 60°. As can be seen, the spectral curves are similar. The light attenuations and red shifts are slight and can be ignored. A clear view of the spectra in the region of λ_c is shown in the enlarged embedded picture. At a divergence angle of 60°, a blue shift of less than 1 mm occurs. The spectral transmission is the highest because the distance that the light travels in the medium is the shortest (Fig. 4, $L \approx 2.9$ mm). At a divergence angle of 30°, slight red shift and light attenuation occur because the distance that the light travels in the medium is slightly longer than the reference length, t_0 (see Fig. 4, $L \approx 3.015$ mm). At a divergence angle of 45°, the distance that the light travels in the medium is equal to the reference length t_0 (Fig. 4, $L = 3$ mm). However, the reflection factor at a divergence angle of 30° is slightly larger than that at a divergence angle of 45°. Therefore, the spectral transmission at a divergence

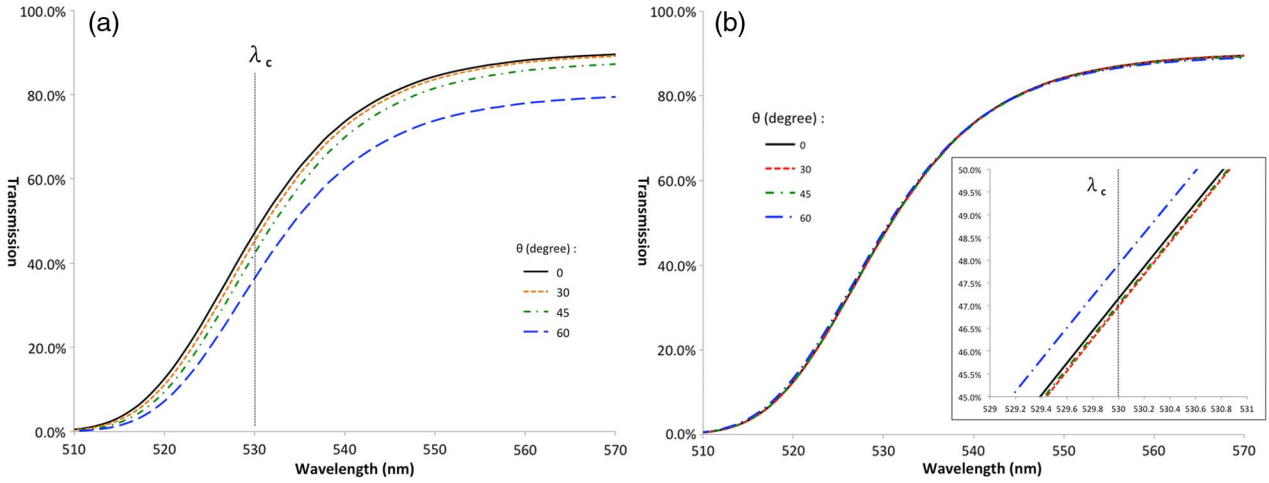

Fig. 5. External transmission curves of (a) the normal filter and (b) the filtering lens at divergence angles of 0°, 30°, 45°, and 60°. The λ_c is the cutoff wavelength of the filter and lens material.

angle of 30° is slightly lower than that at the divergence angle of 45°.

B. Close-Up Lens

A close-up lens for macrophotography was designed by Optalix simulation. It is a magnifying glass optimized for filtering lenses and is placed between the camera lens and the object. The close-up lens decreases the EFL of the camera lens, and therefore provides high magnification capabilities. As shown in Fig. 6, the close-up lens collimates the diverging light rays that originated from the object. It is a symmetrical, double-convex lens with a radius of curvature of 84.5 mm. The lens material is BK7. The inserted filtering lens ($R_c = 172$ mm) shortens the EFL of the close-up lens from 84.5 to 83.9 mm. The close-up lens provides not only a macro-imaging function, but also an aid for the experiment to demonstrate the efficacy of the filtering lens. For the purpose of uniform optical filtering, the close-up lens benefits greatly from the filtering lens.

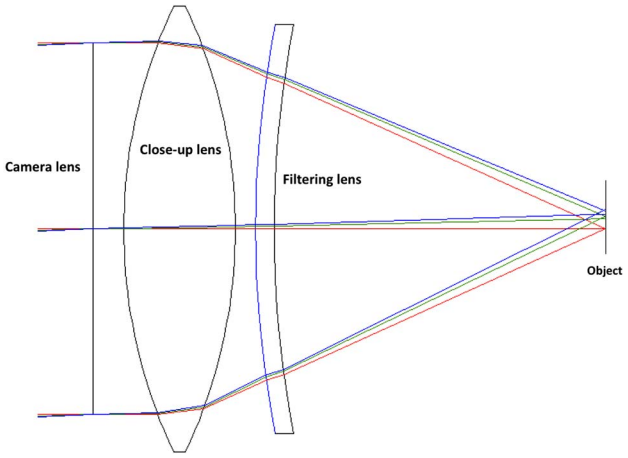

Fig. 6. Illustration of the optical simulation for the close-up lens and filtering lenses.

3. Experimental Measurement

The normal filter, filtering lens, and close-up lens were prepared by precise optical manufacturing processes and tested with the Zygo interferometer. Figure 7(a) shows the lenses used in the experiment. The normal filter in a white mounting served as the reference. It had a uniform thickness of 3 mm± 0.01 mm. The filtering lens in a thin black mounting was used to correct the spectrum aberration. According to the design discussed in Theoretical Analysis, the filtering lens was made into a meniscus with radii of curvature of 172 mm ± 0.05 mm, and a lens center thickness of 3 mm ± 0.01 mm. These two optical components were made of long pass (orange) glass. The close-up lens in a thick black mounting was used for the macro-imaging and to demonstrate the efficacy of the filtering lens. It was formed by a symmetrical double convex with radii of curvature of 172 mm ± 0.05 mm. Figure 7(b) shows the assembly of the ordinary camera lens and the filtering macrolens.

Figure 8 shows the schematic of the experimental setup for the performance test of the filtering macrolens. The close-up lens was screwed onto the front of a camera lens. A digital single lens reflex camera (DSLR) was used for the macro-optical imaging.

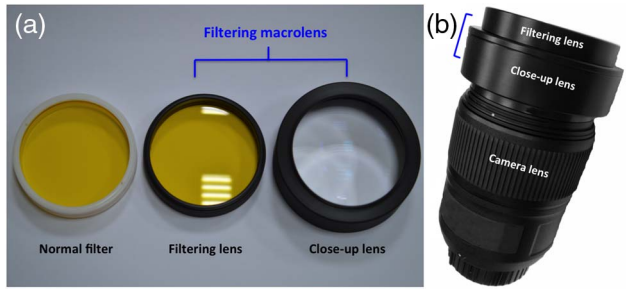

Fig. 7. Overview of the (a) normal filter, filtering lens, and close-up lens and (b) assembly of the camera lens and filtering macrolens (filtering and close-up lenses).

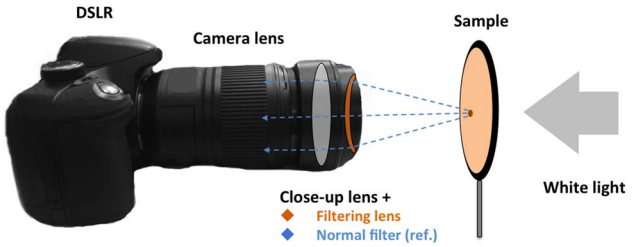

Fig. 8. Experimental setup of the DSLR and the filtering macro-lens for the macro-optical imaging. A long pass glass (OG530) was the sample, illuminated by a uniform white light source.

The focal distance of the camera lens was set manually to infinity because the close-up lens collimates the diverging light beams from the object. A commercial orange filter served as a sample and was illuminated by a uniform white light source. Accordingly, the spectrum of the beams from the object was uniform. The optical setup was calibrated to confirm that the focal plane was precisely located on the surface of the sample.

Figures 9(a) and 9(b) show the optical macro-images captured using the normal filter and the filtering lens, respectively. The relatively strong vignetting effect and color cast are obvious in Fig. 9(a). This result is consistent with the theoretical prediction and represents the spectrum aberration. In contrast, the filtering lens successfully restrains the vignetting effect and color cast in Fig. 9(b). However, a slight vignetting effect is still present in the image. This can be attributed to the original characteristics of the camera lens and the imperfect correction because of the aspherical shape of the filtering lens. For numerical analysis, 30 raw image files were taken individually at various areas of the sample, with both the normal filter and the filtering lens. To decrease the noise coming from the dark currents of the CCD camera and to confirm the reliability of the experiment, every pixel in the 30 acquired images was averaged individually to obtain a normalized image. Thus, two normalized images were each obtained for the normal filter and the filtering lens, for comparison. An image captured by a CCD camera is composed of red (R), green (G), and blue (B) color signals (RGB color model). Figures 9(c) and 9(d) show the R and G values related to the diagonal line of the normalized images for the normal filter and the filtering lens, respectively. No B curve is shown in the diagram because its value is always zero. The slight asymmetry in these curves might be caused by imprecise opto-mechanical components. The curves had been uniformly offset by a constant value to equalize the center brightnesses of the normalized images

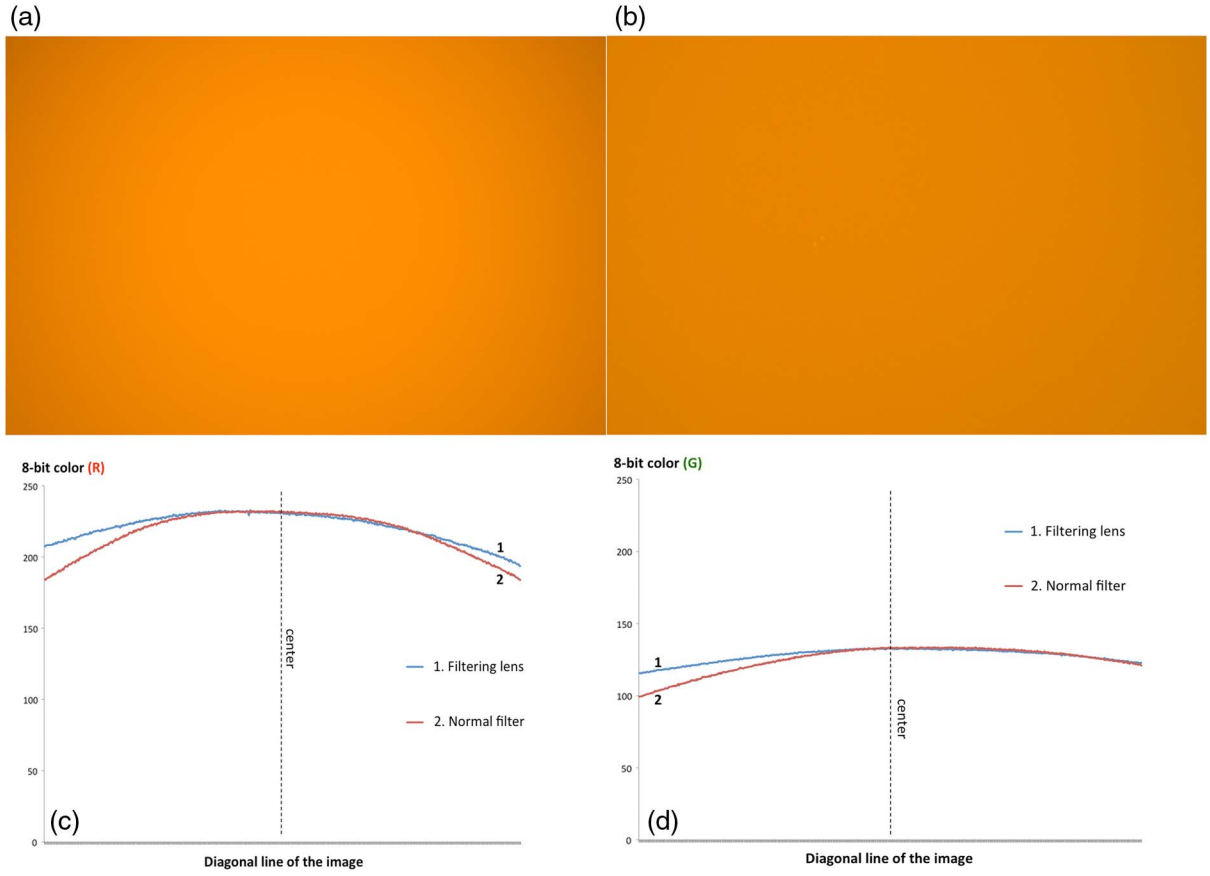

Fig. 9. Optical macro-images captured via (a) the normal filter and (b) the filtering lens. The diagram of (c) the R curves and (d) the G curves related to the diagonal line of the averaged images for the normal filter and filtering lens, respectively. The dotted lines shown in (c) and (d) represent the center of the images.

because the averaging processes led to a slight difference of exposure. After comparing Figs. 9(c) and 9(d), the differences between the center and the border of the R and G curves of the filtering lens were lower than those of the normal filter. This result shows that the filtering lens provided an improved uniformity of brightness and color. The filtering lens thus overcame the spectrum aberration successfully.

4. Conclusion

This study successfully developed a simple, low-cost, and useful filtering macrolens, which is suitable for use infinite conjugate optical systems, compatible with ordinary DSLR camera lenses, and provides favorable spectrum aberration correction and uniform optical density. During the theoretical analysis, a filtering lens with a spherical shape was designed to practically eliminate the OPDs between the light beams traveling through the medium. The close-up lens was designed to achieve macro-optical imaging and provided a means to demonstrate the efficacy of the filtering lens. The experimental results showed that the macro-optical image obtained using the filtering lens had superior spectrum uniformity than that obtained using the normal filter. This indicated that the spectrum-aberration correction of macro-optical images using the filtering lens was demonstrated successfully. This study developed a solution for filter technology and related applications.

References

1. S. S. Zumdahl, *Chemical Principles*, 5th ed. (Houghton, 2003), pp. A18–A20.
2. D. A. Skoog, F. J. Holler, and S. R. Crouch, *Principles of Instrumental Analysis*, 6th ed. (Brooks/Cole, 2007), pp. 336–342.
3. R. B. Tagirow and L. P. Tagirov, "Lambert formula—Bouguer absorption law?" Russ. Phys. J. **40**, 664–669 (1997).
4. Wikipedia, "Beer-Lambert law," http://en.wikipedia.org/wiki/Beer-Lambert_law.
5. Wikipedia, "Mathematical descriptions of opacity," http://en.wikipedia.org/wiki/Mathematical_descriptions_of_opacity#cite_ref-Griffiths9.4.3_2-1.
6. Alex Ryer, *Light Measurement Handbook* (International Light, 1998), p. 14.
7. Steven K. Dew and Robert R. Parsons, "Absorbing filter to flatten Gaussian beams," Appl. Opt. **31**, 3416–3419 (1992).
8. S. O. Kasap, *Optoelectronics and Photonics: Principles and Practices* (Prentice-Hall, 2001), pp. 16–22.
9. H. Abitan, H. Bohr, and P. Buchhave, "Correction to the Beer–Lambert–Bouguer law for optical absorption," Appl. Opt. **47**, 5354–5357 (2008).
10. Wikipedia, "Macro photography," http://en.wikipedia.org/wiki/Macro_photography.
11. Schott, "Longpass filters," http://www.schott.com/advanced_optics/english/products/filteroverviewdetail-longpass.html.
12. Wikipedia, "Close-up filter," http://en.wikipedia.org/wiki/Close-up_filter.
13. H. Eugene, *Optics* (Addison-Wesley, 1998), pp. 111–120.